High Energy Photons From Gamma Ray Bursts

Shlomo Dado[1] and Arnon Dar[2]

ABSTRACT

Emission of high energy (HE) photons above 100 MeV that is delayed and lasts much longer than the prompt MeV emission has been detected from several long duration gamma ray bursts (LGRBs) and short hard bursts (SHBs) by the Compton, Fermi and AGILE gamma ray observatories. In this paper we show that the main observed properties of this HE emission are those predicted by the cannonball (CB) model of GRBs: In the CB model all the observed radiations in a GRB are produced by the interaction of a highly relativistic jet of plasmoids (CBs) with the environment. The prompt X-ray and MeV γ-ray pulses are produced by inverse Compton scattering (ICS) of glory photons - photons scattered/emitted into a cavity created by the wind/ejecta blown from the progenitor star or a companion star long before the GRB- by the thermal electrons in the CBs. A simultaneous optical and high energy emission begins shortly after each MeV pulse when the CB collides with the wind/ejecta, and continues during the deceleration of the CB in the interstellar medium. The optical emission is dominated by synchrotron radiation (SR) from the swept-in and knocked-on electrons which are Fermi accelerated to high energies by the turbulent magnetic fields in the CBs, while ICS of these SR photons dominates the emission of HE photons. The lightcurves of the optical and HE emissions have approximately the same temporal behaviour but have different power-law spectra. The emission of very high energy (VHE) photons above 100 TeV is dominated by the decay of π^0's produced in hadronic collisions of Fermi accelerated protons in the CBs. The CB model explains well all the observed radiations, including the high energy radiation from both LGRBs and SHBs as demonstrated here for GRB 090902B and SHB 090510.

Subject headings: gamma rays: bursts

[1]dado@phep3.technion.ac.il
Physics Department, Technion, Haifa 32000, Israel

[2]arnon@physics.technion.ac.il
Physics Department, Technion, Haifa 32000

1. Introduction

During nearly 20 years after the launch of the Compton Gamma Ray Observatory (CGRO), the Burst And Transient Source Experiment (BATSE) on board the CGRO has detected and measured light curves and spectra (Kaneko et al. 2008) in the sub-MeV range of several thousands gamma ray bursts (GRBs). Higher-energy observations with the EGRET instrument aboard CGRO were limited to those GRBs which happened to be in its narrower field of view. Its large calorimeter measured the light-curves and spectra of several GRBs in the 1-200 MeV energy range. Seven GRBs were detected also with the EGRET spark chamber, sensitive in the 30 MeV - 10 GeV energy range. The EGRET detections indicated that the spectrum of bright GRBs extends beyond 1 GeV (Hurley et al. 1994) with no evidence for a spectral cut-off (see, e.g., Dingus 1995, 2001 and references therein). However, a few GRBs, such as 940217 (Hurley et al. 1994) and 941017 (Gonzalez et al. 2003), showed evidence that the high energy component has a slower temporal decay than that of the sub-MeV emission, suggesting that, at least in some cases, it is not a simple extension of the main component, but originates from a different emission mechanism and/or region. This has been confirmed recently by observations of high energy photons in the 30 MeV - 300 GeV range from several GRBs with the AGILE (GRB 080514B: Giuliani et al. 2008, GRB 090510: Giuliani et al. 2009) and the Fermi large area telescope (LAT) (e.g., GRB 080916C: Abdo et al. 2009a, GRB 090902B: Bissaldi et al. 2009 and GRB 090510: Ghirlanda et al. 2009). The arrival times of the high energy photons did not coincide with the times of the brightest peaks seen at hard X-rays and MeV γ-rays. Also the high energy emission lasted much longer time than that of the prompt keV-MeV emission.

The detection of higher energy gamma rays is affected by pair production in their collisions with the extragalactic infrared background light (Nikishov 1961) resulting in an absorption which is a strong function of redshift and energy. Recent estimates (Primack et al. 2005), validated by HESS observations (Aharonian et al. 2006) predict an optical depth of roughly unity to 500 GeV photons emitted at a redshift $z = 0.2$ and to 10 TeV photons at $z = 0.05$. The average redshifts of LGRBs and SHBs are much larger, $z = 2.2$ and $z = 0.5$, respectively. Despite of the strong attenuation of high energy gamma rays in the intergalactic medium (IGM), there have been several claims in the past of detections at the 3 sigma level of TeV gamma-rays from GRBs (see, e.g., Atkins et al. 2003 and references therein). However, more recently, no GRB was conclusively detected in the range 100 GeV to 100 TeV by the ground based water Cherenkov detector Milagro and by the air Cherenkov telescopes MAGIC, Whipple, HESS and VERITAS. Moreover in all previous cases of reported detection of TeV gamma-rays from a GRB, the GRB redshift was not known. If their redshifts are similar to those of ordinary GRBs then their TeV gamma-rays are strongly absorbed by the extragalactic background light (EBL), implying that the TeV emission if detected must be

extraordinarily energetic, i.e., with a much larger fluence than that emitted in X-rays and MeV γ-rays.

Most theoretical models of high energy photon emission in GRBs relied on the standard fireball models of GRBs (for recent reviews see, e.g., Piran 2005; Mészáros 2006; Zhang 2007). In these models, synchrotron radiation of electrons accelerated by 'internal shocks' in collisions between conical shells ejected by the GRB's central engine produces the prompt GRB emission and a blast wave (external shock) driven into the circumburst medium generates their afterglow. The high energy radiation was suggested to be produced either by inverse Compton scattering of the synchrotron radiation (the so called 'synchrotron self Compton mechanism') by the shock-accelerated electrons (e.g., Dermer et al. 2000), by the decay of π^0 photo produced in collisions of shock accelerated hadrons with synchrotron photons in the expanding fireball (Waxman & Bahcall 1997), or by synchrotron radiation from ultra high energy protons (Totani 1998) allegedly accelerated in the GRB fireball (Waxman 1995; Milgrom & Usov 1995; Vietri 1995). All these models that were based on the standard fireball model of GRBs predict simultaneous emissions at all energy bands. This is in conflict with the observed delayed emission of the high energy photons that lasts much longer.

In the cannonball (CB) model (see e.g. Dado, Dar & De Rújula, hereafter DDD, 2009a,b and references therein), GRBs and their afterglows (AGs) are produced by bipolar jets of highly relativistic plasmoids (CBs) ejected in violent stellar processes. The prompt MeV γ-rays and hard X-rays are produced by inverse Compton scattering (ICS) of glory photons - photons emitted/scattered into a cavity formed by the wind/ejecta puffed by the progenitor or a companion star long before the GRB. Synchrotron radiation (SR) emitted from the electrons of the ionized wind/ejecta that are swept into the CBs and are Fermi accelerated by their turbulent magnetic fields dominates their 'prompt' optical emission (e.g., DDD2009a and references therein) which begins when the CBs reach the wind/ejecta. In this paper we show that in the CB model ICS of this SR (e.g., Dado & Dar 2005) dominates the HE emission from long GRBs and SHBs. This HE emission begins simultaneously with the 'prompt' optical emission that lags after the prompt X-ray and MeV γ-ray emission and lasts much longer, has the same lightcurve as the optical emission but with a power-law spectrum that is identical to that of the X-ray emission. It describes well the HE observations, as demonstrated in the paper for GRB 090902B and SHB 090510.

Because of the Klein-Nishina effect, $E^2\, dn/dE$ of ICS of the prompt SR in GRBs peaks near 10 TeV and is cutoff at a few tens of TeV when the rate of synchrotron energy losses by electrons in the CBs exceeds the rate of energy gain by Fermi acceleration. The prompt decay of π^0's produced in the collisions between the Fermi accelerated nuclei and the ambient matter in the CBs produces a power-law spectrum that extends to much higher energies

where it dominates the HE emission. However, like in blazars, the observed flux of TeV photons from distant GRBs and SHBs is stronglyly suppressed by pair production in collisions with the extragalactic background photons and only relatively nearby GRBs and SHBs might be detected in TeV photons by the large ground based HE gamma ray telescopes such as HESS, MAGIC and VERITAS.

2. The CB model

In the cannonball (CB) model (Dado, Dar & De Rújula (hereafter DDD) 2002; Dar & De Rújula (hereafter DD) 2004; DDD2009a,b and references therein) GRBs and their AGs are produced by bipolar jets of highly relativistic CBs of ordinary matter which are ejected (Shaviv & Dar 1995, Dar & Plaga 1999) in the birth of neutron stars or black holes in core-collapse supernova (SN) explosions (long GRBs) akin to SN 1998bw (Galama et al. 1998), and in the merger of neutron stars and/or phase transition in compact stars (short hard bursts). Their prompt MeV γ-rays and hard X-rays are produced by the thermal electrons in the CBs' plasma via inverse Compton scattering (ICS) of glory photons - photons emitted/scattered into a cavity created by the wind/ejecta blown from the progenitor star or a companion star long before the GRB. Slightly later when the CBs encounter the wind/ejecta, and afterwards when the CBs coast through the interstellar medium (ISM) sorounding it, the electrons of the ionized gas in front of them that are swept in and Fermi accelerated by the CBs' turbulent magnetic fields emit synchrotron radiation (SR) which dominates the 'prompt' optical emission and the broad band afterglow emission. ICS of the SR radiation by these electrons and the decay of π^0's produced in collision between the swept-in wind and ISM protons and the ambient CB protons produce the 'prompt' high energy emission simultaneously with the optical emission. Within the CB model, the burst environment as illustrated in Fig. (1) and the above radiation mechanisms, which are summarized in Table 1, suffice to provide a sufficiently accurate description of the observed radiations from GRBs at all times and all detected wavelengths.

3. ICS of self produced SR

3.1. Self produced SR

When a CB encounters the wind/ejecta which was blown by the progenitor star long before the GRB, it sweeps in the ionized matter in front of it. The swept in electrons and nuclei that in its rest frame enter it with a Lorentz factor γ equal to that of the bulk motion

of the CB, are isotropized and Fermi accelerated in the CBs by its turbulent magnetic field. They emit SR with an early-time lightcurve in the observer frame (DDD2009a) :

$$F_\nu[t] \propto \frac{e^{-a/t}\, t^{1-\beta}}{t^2 + t_{exp}^2}\, \nu^{-\beta} \rightarrow t^{-(1+\beta)}\, \nu^{-\beta}\,, \tag{1}$$

where $t = T - T_i$, T is the observer time after trigger and T_i is the observer time when the CB reaches the wind/ejecta. The optical band is initially well below the 'bend' frequency (DDD2009a). Consequently, $\beta_O \approx 0.5$ and the 'prompt' optical flare that follows an ICS keV-MeV pulse/flare, decays like $F_\nu \propto t^{-1.5}\, \nu^{-0.5}$.

3.2. ICS in the Thomson and Klein-Nishina regimes

The differential cross section for Compton scattering of a photon with energy E_γ from an electron at rest was calculated by Klein & Nishina in 1929. In the electron's rest frame it is given by,

$$\frac{d\sigma}{d\Omega} = \frac{1}{2}\left(\frac{e^2}{m_e\, c^2}\right)^2 (k - k^2\, sin^2\theta + k^3)\,, \tag{2}$$

where

$$k(E_\gamma, \theta) = \frac{1}{1 + \frac{E_\gamma}{m_e\, c^2}\,(1 - cos\theta)} \tag{3}$$

The final energy of the scattered photon is, $k\, E_\gamma$.

In the Thomson regime where $E_\gamma \ll m_e\, c^2$, and then $k \approx 1$, $d\sigma/d\Omega \propto (1 + cos^2\theta)$ and the mean final energy of a photon that suffered an ICS by an electron of energy E_e is $(4/3)\,(E_e/m_e\, c^2)^2\, E_\gamma$. A power-law distribution of Fermi accelerated electrons $dn_e/dE \propto E^{-p}$ generates through ICS a power-law distribution of scattered photons with $E^2\, dn_\gamma/dE \propto E^{-(p-3)/2}$, where $p \approx 2.2$ well below the electron cooling energy and $p \approx 3.2$ well above it.

In the Klein-Nishina (KN) regime where $E_\gamma > m_e\, c^2$ in the electron rest frame, $k\, E_\gamma \sim m_e\, c^2$, $\sigma_{KN} \propto 1/E_e$, and the mean energy of a photon that suffered an ICS by an HE electron is approximately E_e. In the KN regime, a power-law distribution of electrons $dn_e \propto E^{-(p+1)}\, dE$ generates by ICS of self produced SR a power-law distribution of scattered photons with $E^2\, dn_\gamma/dE \propto E^{-(p+1)/2)}$. In particular, for a distribution of Fermi accelerated elecctrons that suffer a fast radiative cooling, $p \approx 3.2$ and the scattered photons in the lab frame have a power-law distribution,

$$E^2\, \frac{dn_\gamma}{dE} \propto E^2\, \frac{dn_e}{dE}\, \sigma_{KN} \sim E^{-(p+1)/2} \sim E^{-1.6}\,. \tag{4}$$

3.3. SSC in GRBs

Like in blazars, the radiation produced by ICS of self produced SR, the so called 'SSC emission', is Doppler boosted by the CB relativistic motion and extends almost to TeV energies above which it is suppressed by the Klein-Nishina effect. Roughly, the SSC energy flux $\nu\,F_\nu$ in the Thomson regime first increases with energy like $E^{(3-p)/2}$, where $p{\approx}2.2$ until $E\sim E_p{\approx}2\,m_e\,c^2\,\gamma\,\delta/3\,(1+z)$, then it changes into a plateau/shallow decrease like $E^{-(p-2)/2}$, due to the cooling break in the HE electron distribution, until it enters the Klein-Nishina regime where it decreases like $E^{-(p+1)/2}$. For typical GRBs (DDD2009a) where $\delta{\approx}\gamma{\sim}1000$ and $1{+}z{\sim}3.2$, the peak of the unabsorbed energy flux density is around $E_p{\sim}100$ GeV. In very luminous GRBs, the peak energy E_p of the SSC may approach TeV, which is above the LAT energy range, and then could be detected only in relatively very nearby GRBs where absorption in the IGM by pair-production can be neglected. Beyond the peak-energy, the SSC is cut off at an energy $E_c{=}m_e\,c^2\,\gamma_{e,max}\,\gamma/(1{+}z)$ by the cut-off in the electron spectrum at $\gamma_{e,max}=\sqrt{6\,e/\sigma_T\,B_{eq}}$ in the CB rest frame when the energy loss-rate by SR exceeds the rate of Fermi acceleration by the strong equipartition magnetic field $B_{eq}{\approx}\sqrt{4\,\pi\,n\,m_p\,c^2}\,\gamma$ generated in the CB by its collision with the wind/ejecta ($n\,m_p$ is the density of the wind and $\sigma_T\ {\approx}0.665\times10^{-24}\,\mathrm{cm}^{-2}$ is the Thomson cross section).

In the CB model each GRB pulse have a sub-MeV energy flux density which is well approximated by an exponentially cutoff power-law $F_E{\propto}E^{-\beta_g}\,e^{-E/E_p(t)}$ where $\beta_g{\sim}0$, $E_p(t){\sim}E_p(0)\,t_p^2/(t^2{+}t_p^2)$, and t is the time after the beginning of the pulse (e.g. DDD2009a and references therein). Towards the end of each ICS pulse simultaneous 'prompt' optical and HE emissions begin. They have a power-law spectrum $F_\nu{\propto}\nu^{-\beta}$, with $\beta{\sim}0.5$ in the optical band and $\beta_O\,\leq\,\beta\,\leq\,\beta_X$ in the LAT band. The time integrated spectrum over a single GRB pulse (or several unresolved GRB pulses) appears to be an exponentially cutoff power-law spectrum with E_p in the keV-MeV range plus a power-law component. The power-law component dominates both at low energies because $\beta_g{\lesssim}0$ whereas $\beta_{OX}\sim0.8$, and at high energies because of the exponential cut-off of the spectrum of the prompt MeV emission.

4. External ICS of prompt GRB photons

The thermal electrons (and the Fermi accelerated ones) in the CBs that have the CB bulk motion Lorentz factor γ in the observer frame can boost by ICS the energy of prompt sub-MeV GRB photons which suffer Compton scattering in the wind and are overtaken shortly by the CBs. However, this mechanism is strongly suppressed by the Klein-Nishina effect for GRB photons whose energy is above${\sim}1$ eV and thus does not contribute effectively to the production of HE photons.

5. Hadronic production of HE photons by thermal protons

The radiative decay of π^0's produced in collisions between thermal CB nuclei and wind nuclei produce sub-TeV γ-rays. Neglecting magnetic deflections of the CB nuclei in the wind, the equivalent isotropic energy of sub-TeV γ's produced that way is given by,

$$E_{iso}^{HE} \sim 0.08\, E_{CB}\, \sigma_{in}\, N_{wind}\, \delta^2\,, \tag{5}$$

where 0.08 is the fraction of the incident kinetic energy of protons that is carried by the π^0's produced in HE pp collisions, $\sigma_{in} \approx 40$ mbarn is the HE pp inelastic cross section, $N_{wind} \sim 10^{21\pm1}\mathrm{cm}^{-2}$ is the typical column density of the GRB environment as inferred from the spectral measurement with the Swift X-ray telescope (XRT), $E_{CB} \sim 10^{50}$ erg is the canonical kinetic energy of a CB ejected in core collapse supernovae which produce GRBs (DD2004), and δ^2 is the relativistic beaming factor in the CB model. These numbers yield $E_{iso}^{\pi^0} \sim\ 3.2\times10^{50\pm1}$ erg, which is much smaller than the typically observed equivalent isotropic gamma ray energy of the HE component in GRBs with a detectable HE emission.

6. Hadronic production of HE photons by Fermi accelerated protons

The wind nuclei which enter a CB are Fermi acceleration through magnetic deflections by the turbulent magnetic fields in the CB. Their total path-length inside a CB before they escape can be much larger than their mean free path for hadronic collisions. In that case, a fraction ~ 0.08 of the CB's kinetic energy is converted to HE gamma rays through π^0 production and decay and a similar fraction is converted through gamma ray production in the hadronic showers by radiative decays, SR from charged leptons and ICS of the SR in the CBs . Due to Feynman scaling, these HE γ-rays have a power-law spectrum with a power-law index equal to that of the Fermi accelerated nuclei, i.e., $dn_\gamma/dE \propto E^{-2.2}$. The total equivalent isotropic energy is then bounded by a fraction $0.08 \lesssim k \lesssim 0.25$ of the kinetic energy of the jet which is converted into HE γ-rays that are beamed into a solid angle $\sim \pi\,\delta^{-2}$. This yields the upper limit:

$$E_{iso}^{HE} \leq k\ \times 10^{56}\ \left[\frac{E_{CB}}{10^{50}\,\mathrm{erg}}\right]\ \left[\frac{\delta}{1000}\right]^2\ \mathrm{erg}. \tag{6}$$

In the CB model, the exact value of k and consequently of E_{iso}^{HE} and the early-time lightcurve of the HE 'hadronic' γ ray emission before the CBs enter the ISM are strongly model-dependent and involve many unknown parameters. However, when the jet enters the ISM, the lightcurve is similar to that of the X-ray afterglow until the jet break/bend (DDD2009a).

Roughly, the same spectra, E_{iso}, and lightcurves are expected for the HE γ-ray emission and the ν_μ emission in GRBs from hadronic production and decay of π^0 and $\pi^\pm$, respectively.

7. Comparison with observations

The rapid localization of a few degrees, which is delivered by the Fermi GBM, is not precise enough for a rapid localization and follow-up by current optical telescopes. The localization of the HE emission detected by the LAT seems good for optical follow-up but, so far, it is delivered with a large delay compared to the GRB itself. Consequently, the coincidence in time between the HE emission and the optical emission and the similarity between their light curves, which are predicted by the CB model, cannot be tested yet in individual GRBs. However, the decay of the prompt optical flares seems to satisfy the CB model prediction (DDD2009) of a power-law decay with an index α=1+$\beta_0 \sim$ 1.5. Such a power-law decay seems to agree with the observed power-law decay of the HE emission that was detected by the Fermi LAT in 11 GRBs so far (see, e.g., Ghisellini1, Ghirlanda & Nava 2009). Moreover, the spectrum of the HE emission which was measured by the Fermi LAT seems to be described well by a power-law with a spectral index which satisfies, admittedly within large errors, the relation, $\Gamma_{LAT} \approx \Gamma_X$, predicteby the CB model, where Γ_X is the photon index of the *late-time X-ray AG*. This is shown in Table 2 and in Fig. 2 where we plotted the ratio Γ_{LAT}/Γ_X for 7 GRBs that were observed both by the Fermi LAT and by the Swift XRT. Note that the average ratio is consistent with 1 with a small error unlike large error in this ratio for the individual GRBs. Below we compare in detail the CB model predictions and the observations of two representative GRBs with HE emission that was detected by LAT, the long GRB 090902B and SHB 090510.

7.1. GRB 090902B

Observations: The Fermi Gamma-ray Burst Monitor (GBM) triggered on and localized the bright burst GRB 090202B on 2009 September 2 at 11:05:08.31 UT. The burst had a multi-peak structure with the brightest peak around 14 sec after trigger. It was also detected by the INTEGRAL and Suzaku satellites. The sub-MeV ended approximately 25 seconds after trigger. Emission above 100 MeV was detected by the Fermi LAT up to 1k sec after the GBM trigger when the Earth's limb was starting to enter its field-of-view, with 39 photons above 1 GeV (de Palma et al. 2009). The highest energy photon had E= 33.4 +2.7/-3.5 GeV and arrived 82 seconds after the GBM trigger. The emission declined like $t^{-1.5}$ until the LAT observations were interrupted by entry of the Earth's limb into its field of view, but analysis of data an hour after trigger, when the source location was again unocculted, showed that any later emission lied below the LAT sensitivity (Bissaldi et al. 2009). At a redshift of z=1.822 (Cucchiara et al. 2009), the fluence of $(4.36 \pm 0.06) \times 10^{-4}\,\mathrm{erg\,cm^{-2}}$ during the first 25 seconds of the prompt emission yields $E_{iso}=(3.63 \pm 0.05) \times 10^{54}$ erg isotropic equivalent

γ-ray energy in the 10 keV-10 GeV range.

The X-ray follow-up observations with the Swift X-ray telescope (XRT) started only 12.5 hours after the GBM trigger. The measured X-ray spectrum can be fit by an absorbed power-law model with a photon index of $\Gamma = 2.1 \pm 0.3$ and a rest frame column density of $(3.4 \pm 0.9) \times 10^{22}\,\mathrm{cm}^{-2}$ at z=1.822 in addition to the Galactic column density in the direction of the burst (Stratta et al. 2009).

The earliest ground-based optical observations were obtained only $\sim$1.4 h after trigger by ROTSE-IIIa (Pandey et al. 2009). The burst was later detected also in the optical, infra red and radio.

Interpretation: From the LAT detection of the highest energy photon of 11.16 (+1.48/-0.58) GeV during the prompt phase Bissaldi et al. (2009) inferred a minimum value of the bulk Lorentz factor $\gamma(0) \geq 1000$ of the source using the flux variability time scale of 53 ms and the constraint that the opacity for $e^{\pm}$ pair-production in the source is less than unity so that such photons can escape outside the source (Fenimore et al. 1993). A similar value was derived for GRB 080916C (Abdo et al. 2009a). *Such values of the bulk motion Lorentz factor of the jet of CBs were long advocated by the CB model (e.g., DDD2002; DD2004) and were used to explain the typical photon energy and isotropic equivalent energy of long GRBs.* For standard candle GRBs, the largest observed values of E_{iso} and E_p are obtained when the GRBs are viewed from very near axis, i.e., with a viewing angle $\theta^2 \ll 1/\gamma(0)^2$. In that case the Doppler factor of the CBs is $\delta(0) \approx 2\,\gamma(0)$. In the CB model, the isotropic gamma ray energy of such GRBs is (DD2004): $E_{iso} \approx 8 \times 10^{52}\,(\delta(0)/1000)^3\,N_{CB}$ erg. It yields $E_{iso} \geq 3.2 \times 10^{54}$ erg for a jet of N_{CB}=5 canonical CBs (producing the 5 main peaks in the lightcurve of GRB 090902B) and $\delta(0) = 2\,\gamma(0) \geq 2000$. This value agrees with the value $E_{iso} \approx 3.63 \times 10^{54}$ erg that was inferred by Bissaldi et al. (2009) from the Fermi measurements.

The time-averaged spectrum in the 100-1000 keV during the 25 sec of the sub-MeV GRB prompt phase was well fitted by a power-law with photon index Γ=0.91+/-0.10 and an exponential cutoff with E_p=885+/-0.39 keV (Terada et al. 2009). The photon index β_g=Γ-1=-0.09+/-0.10 is consistent with the CB model expectation $\beta_g \sim 0$. The rest frame value of the peak energy $(1+z)\,E_p = 2550 \pm 112$ keV is also consistent with that expected in the CB model as shown in Fig. (3): it satisfies the so called 'Amati correlation' which follows from the CB model and was predicted (see e.g., DDD2007 and references therein) long before it was discovered.

The GRB peaks are not well resolved in the Fermi GBM data and do not allow a stringent test of the CB model predictions for the temporal and spectral behaviour of the individual prompt MeV peaks/flares.

Due to insufficient statistics, also the early-time lightcurve of the HE emission, which was measured by the Fermi LAT, was not well resolved into separate peaks. However, as shown in Fig. (4), it is well described by Eq. (**??**) assuming a single effective CB with the parameters listed in Table 3. Note that its predicted decline, until taken over by its shallow decay of the SSC in the ISM is well described by the expected decline, $F_\nu \propto t^{-1\beta_O}$ (see Eq. (**??**). Also the photon spectral index of the HE emission as measured by Bissaldi et al. 2009, $\Gamma = 1.93 \pm 0.03$, as predicted, is equal within errors to the measured spectral index in the X-ray band, $\Gamma_X = 2.1 \pm 0.3$ inferred by Stratta et al. (2009) from the Swift XRT data.

No early-time optical data is available to test the CB model prediction that the prompt optical emission and the high energy emission have the same temporal behaviour. In the CB model each prompt MeV peak/flare has a delayed HE peak that decays asymptotically like $t^{-1-\beta_O}$ and the time-lag between the prompt MeV emission and the high energy emission in each pulse is of the order of the pulse width, while the bulk of the high energy emission is delayed typically by a time comparable to the duration of the MeV component. There are indications for such correlations in the data obtained by the Fermi LAT and GBM on GRB 090902B and 080916C.

In the CB model, the observed late time behaviour of the lightcurve of the unabsorbed X-ray afterglow is described by a power-law $F_\nu \propto t^{-\alpha_X}\, \nu^{-\beta_X}$ with $\alpha_X = \beta_X + 1/2$. A best fit to the Swift XRT data shown in Fig. (5) yields $\alpha_X = 1.42 \pm 0.1$. This value is consistent within errors with $\alpha_X = 1.6 \pm 0.3$ expected from the spectral index $\beta_X = 1.1 \pm 0.3$ inferred by Stratta et al. (2009) from the Swift XRT data.

7.2. SHB 090510

Observations: SHB 090510 is a short/hard burst at redshift z=0.903 (Rau et al. 2009) detected by Fermi (Guiriec et al. 2009), AGILE (Longo et al. 2009), Swift (Hoversten et al. 2009), Konus-Wind (Golenetskii et al. 2009) and Suzaku (Ohmori et al. 2009). The Fermi GBM triggered on a precursor while the main emission episode started $\sim$ 0.5 sec after trigger and lasted $\sim$ 0.2 sec. Its lightcurve consists of 7 main peaks. The emission detected by the Fermi LAT started 0.65 s after the trigger and lasted $\sim$ 200 sec. The photon with the highest energy of 31 ± 3 GeV arrived 0.829 sec after trigger (Abdo et al. 2009b). The equivalent isotropic gamma ray energy before the onset of the high energy emission was E_{iso}=(3.91 -0.88/+1.91)$\times 10^{52}$ erg. The time integrated photon spectrum measured by AGILE (Giuliani et al. 2009) was fitted with an exponentially cutoff power-law with a photon power-law index Γ=0.65 (-0.32/+0.28) and a cutoff energy E_c=2.8 (-0.6/+0.9) MeV (rest frame peak energy E_p=7.19 (-1.54/+2.31) MeV). The time integrated spectrum between

0.5 and 1 sec after trigger was best fitted by adding a second component -a power-law component with a photon index $\Gamma = 1.62 \pm 0.03$- and resulted with $E_p = 3.9 \pm 0.3$ MeV and $E_{iso} = (1.08 \pm 0.06) \times 10^{53}$ erg (Abdo et al 2009b). The high-energy spectral component accounts for $\sim$ 37% of the total fluence. The bulk of the photons above 30 MeV arrived 258 ± 34 ms later than those below 1 MeV.

Interpretation:

The detection of a 31 GeV photon during the first second sets the highest lower limit on the bulk motion Lorentz factor of the source, $\gamma > 1200$ (Abdo et al. 2009b). This limit is consistent with the typical value $\gamma(0) \sim 1400$ advocated by the CB model for ordinary SHBs (DDD2009b). The large value of E_p probably requires $\gamma(0) \sim 2000$ and a small viewing angle $\theta^2 \ll 1/[\gamma(0)]^2$ implying $\delta(0) \approx 2\,\gamma(0)$ and E_{iso} larger roughly by a factor 23 than 5×10^{51} erg, the mean E_{iso} of SHBs.

Due to insufficient statistics, the early-time lightcurve which was measured by the Fermi LAT cannot be resolved reliably into separate HE peaks. The lightcurve of the blended peaks inferred from the LAT measurements is well described by Eq. (**??**) for a single effective CB with the parameters listed in Table 3 as shown in Fig. (**??**). Also the photon spectral index of the HE emission as measured by Giuliani et al. (2009), $\Gamma = 1.58$ (-0.11,+0.13), and by Bissaldi et al. (2009), $\Gamma = 1.62 \pm 0.03$, is roughly within errors that of the spectral index $\Gamma_X = 1.792$ (+0.071/-0.051) inferred by Evans et al. (2009) from the Swift XRT data. No early-time optical data is available to test the CB model prediction that the prompt optical and high energy emissions have the same temporal behaviour. The two spectral components (a prompt MeV cutoff power-law component and a delayed HE power-law component), show a significant temporal correlation (Abdo et al. 2009b) as expected in the CB model. Lag-times within the MeV band and the HE band were not detected, as expected in the CB model (DDD2009b). The bulk of the photons above 30 MeV arrived $258 \pm$ 34 ms later than those below 1 MeV. This time lag is comparable to the duration of the sub-MeV emission, as expected in the CB model.

In the CB model the asymptotic decline of the X-ray afterglow in $n \propto 1/(r-r_c)^2$ density beyond r_c is given by $F_\nu \propto t^{-\alpha}\,\nu^{-\beta}$ with $\alpha = \beta + 1 = \Gamma$ (e.g., Eq. 32 in DDD2009b). The Swift XRT lightcurve repository (Evans et al. 2009) reports $\Gamma = 1.792$(+0.071/-0.051) from a spectral analysis of the X-ray afterglow, in good agreement with the index $\alpha = 1.89 \pm 0.06$ of the best fit power-law decline beyond 1100 sec after trigger (see Fig. (**??**)).

8. Conclusions

In the cannonball (CB) model, high energy emission from GRBs and SHBs is a natural consequence of the model. The dominant leptonic and hadronic emission mechanisms are ICS of SR by Fermi accelerated electrons in the collision of the jet of highly relativistic CBs with the wind/ejecta blown from the progenitor or companion star long before the GRB, and the decay of π^0 produced in hadronic collisions between the CB nuclei and the nuclei of the hadronic matter (ejecta/wind/ISM) that the jet passes through. The main predictions of the model for the early-time high energy emission are:

- Each prompt keV-MeV pulse is followed by a delayed HE emission which lasts much longer.
- The HE emission coincides in time with the optical emission.
- The light curve of the HE emission is roughly proportional to that of the unextinct optical emission. The decay of both the 'prompt' optical and the HE emissions is a power-law with an index α=1+$\beta_0 \sim 1.5$.
- The spectrum of the HE component is a simple power-law with a spectral index approximately equal to that of the X-ray afterglow, i.e., $\Gamma_{LAT} \approx \Gamma_X$.
- The HE emission extends to very high energies, where the observed radiation is strongly attenuated by e^+e^- pair productin in the EBL.
- The equivalent isotropic energy of the HE component in bright GRBs can reach, and even exceed that in the sub-MeV range.
- The neutrino counterpart of the hadronic emission of HE γ-rays from the most luminous GRBs is barely detectable in km^3 underwater/under-ice Cherenkov neutrino telescopes (DD2008).

These predictions are consistent with the present available data on high energy emission from GRBs obtained from the gamma ray satellites and from the large air, ground and underground Cherenkov telescopes. In particular, the main observed properties of the HE emission measured with the Compton, Fermi and AGILE gamma ray satellites are well reproduced by the CB model as demonstrated in this paper for GRB 090902B and SHB 090510.

An observational proof of the ICS origin of the HE gamma ray emission from GRBs requires simultaneous detections of the prompt optical and HE emissions. It is highly desireable that the LAT team improves their automatic analysis, in order to deliver a GRB

position within a few seconds after the LAT detection. Even a few tens of seconds will be very useful. This will provide a stringent test of models of HE emission from GRBs (and from other HE transient sources such as blazars, microquasars, pulsars, etc) and help pin down their production mechanism. Extremely optically-luminous GRBs, such as GRB 080319 where the prompt optical emission was resolved into individual flares (Racusin et al. 2008), may show that also the prompt high energy emission consists of HE flares which are associated with and follow promptly each individual keV-MeV pulse, as expected in the CB model.

REFERENCES

Abdo, A. A., et al. 2009a, Science, 323, 1688

Abdo, A. A., et al. 2009b, arXiv:0908.1832

Aharonian, F., et al. 2006, MNRAS, 371, 1705

Atkins, R., et al. 2003, ApJ, 583, 824

Bissaldi, E., et al. 2009, arXiv:0909.2470v1

Cucchiara, A., et al. 2009, GCN Circ. 9873

Dado, S. & Dar, A. 2005, ApJ, 627, L109

Dado, S., Dar, A. & De Rujula, A. 2002, A&A, 388, 1079 (DDD2002)

Dado, S., Dar, A. & De Rújula, A. 2007, ApJ. 663, 400 (DDD2007)

Dado, S., Dar, A. & De Rújula, A. 2009a, ApJ, 696, 994 (DDD2009a)

Dado, S., Dar, A. & De Rújula, A. 2009b, ApJ, 693, 311 (DDD2009b)

Dar, A. & Plaga, R. 1999, A&A, 349, 259

Dar, A. & De Rújula, A. 2004, Physics Reports, 405, 203 (DD2004)

Dar, A. & De Rújula, A. 2009, Physics Reports, 466, 179 (DD2008)

de Palma, F., et al. 2009, GCN Circ. 9867

Dermer, C. D., Chiang, J. & Mitman, K. 2000, ApJ, 537, 785

Dingus, B. L., 1995, Astrophys. & Space Sci. 231, 187

Dingus, B. L. 2001, AIP Conf. Proc. 558, 383

Evans, P. A., et al. 2009, MNRAS, submitted, arXiv:0812.3662

Fenimore, E. E., Epstein, R. I. & Ho, C. 1993

Galama, T. J., et al. 1998, Nature, 395, 670

Ghirlanda, G., Ghisellini, G., & Nava, L. 2009, arXiv0909.0016

G. Ghisellini, G., Ghirlanda, G. & Nava, L. 2009, arXiv:0910.2459

Giuliani, A., et al. 2008, A&A, 491, L25

Giuliani, A., et al. 2009, arXiv0908.1908

Golenetskii S., et al. 2009, GCN Circ. 9344

Gonzalez, M. M., et al. 2003, Nature, 424, 749

Guiriec S., et al. 2009, GCN Circ. 9336

Hoversten E. A., et al. 2009, GCN Circ. 9331

Hurley, K., et al. 1994, Nature, 372, 652

Kaneko, Y., et al. 2008, ApJS, 166, 298

Longo F., et al. 2009, GCN Circ. 9343

Mészáros, P. 2006, Rept. Prog. Phys. 69, 2259

Milgrom, M., & Usov, V. 1995, ApJ, 449, L37

Nikishov, A. I. 1961, Zh. Eksp. Teor. Fiz., 41, 549 (English translation:Sov. Phys. JETP 14, 392 [1962])

Ohmori N., et al. 2009, GCN Circ. 9355

Pandey, S. B., et al. 2009 GCN Circ. 9878

Piran, T. 2005, Rev. Mod. Phys. 76, 1143

Primack, J. R. et al. 2005, AIP Conf. Proc. 745, 23

Racusin J. L., et al. 2008, Nature, 455, 183

Rau, A., et al. 2009. GCN Circ. 9353

Shaviv, N. & Dar, A. 1995, ApJ, 447, 863

Stratta, G., DElia, V., & Perri, M. 2009, GCN Circ. 9876

Terada, Y., et al. 2009, GCN Circ. 9897

Totani, T. 1998, ApJ, 502, L13

Vietri, M. 1995, ApJ, 453, 883

Waxman, E. 1995, Phys. Rev. Lett. 75, 386

Waxman, E. & Bahcall, J. N. 1997, Phys. Rev. Lett., 78, 2292

Zhang, B. 2007, ChjAA, 7, 1

Table 1. The dominant particle populations in the CBs and their dominant radiation mechanisms during the prompt/early-time emission phase in GRBs

CB Population	Origin	Target	Mechanism	Energy Band
Thermal e's	CB	Glory photons	ICS	keV-MeV
Fermi accelerated e's	CB-Wind Collision	CB Magnetic Field	SR	UVOIR
Fermi accelerated e's	CB-Wind Collision	Self SR	ICS (SSC)	HE
Thermal p's	CB	Wind/Ejecta	π^0 decay	Sub-TeV
Fermi accelerated p's	CB-Wind Collision	CB Nuclei	π^0 decay	UHE

Table 2. The dominant particle populations in the CBs and their dominant radiation mechanisms during the prompt/early-time emission phase in GRBs

GRB	T_i [s]	T_f [s]	Γ_{LAT}	Γ_X
080825C	0	200	1.96 ± 0.30	
080916C	0	200	2.09 ± 0.12	2.03 (+0.43, -0.43)
081024B	0	5	1.64 ± 0.47	
090217	0	1	2.22 ± 0.40	
090323	0	400	2.05 ± 0.20	1.96 (+0.24, -0.21)
090328	0	100	1.76 ± 0.35	1.82 (+0.23, -0.31)
090510	0	7	2.15 ± 0.12	1.79 (+0.071, -0.051)
090626	0	600	1.70 ± 0.12	
090902B	0	320	2.32 ± 0.16	2.24 (+0.25, -0.25)
090926A	0	25	2.34 ± 0.14	2.15 (+0.072, -0.071)
091003	0	100	1.85 ± 0.25	1.87 (+0.15, -0.16)

Table 3. The parameters of the CB model fitted lightcurve of the prompt/early-time HE emission and the late X-ray AG from GRB 090902B and SHB 090510.

GRB	T_i [s]	t_{exp} [s]	a [s]	A	β_O	β_{HE}	β_X
GRB 090902B	0.63	6.28	0.14	0.118 $cm^{-2}\,s^{-1}$	0.51	0.93 ± 0.03	1.10 ± 0.30
SHB 090510	0.662	0.227	0.0167	36.4 s^{-1}	0.54	0.62 ± 0.03	0.79 ± 0.07

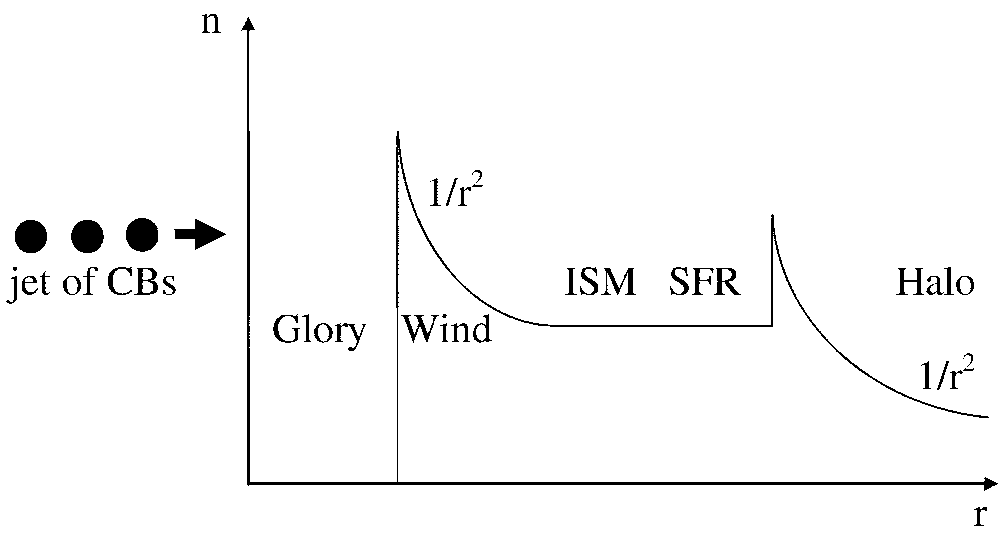

Fig. 1.— Schematic illustration, not in scale, of the typical environment encountered by a highly relativistic jet ejected in core collapse SN that escapes from the star formation region into the galactic halo.

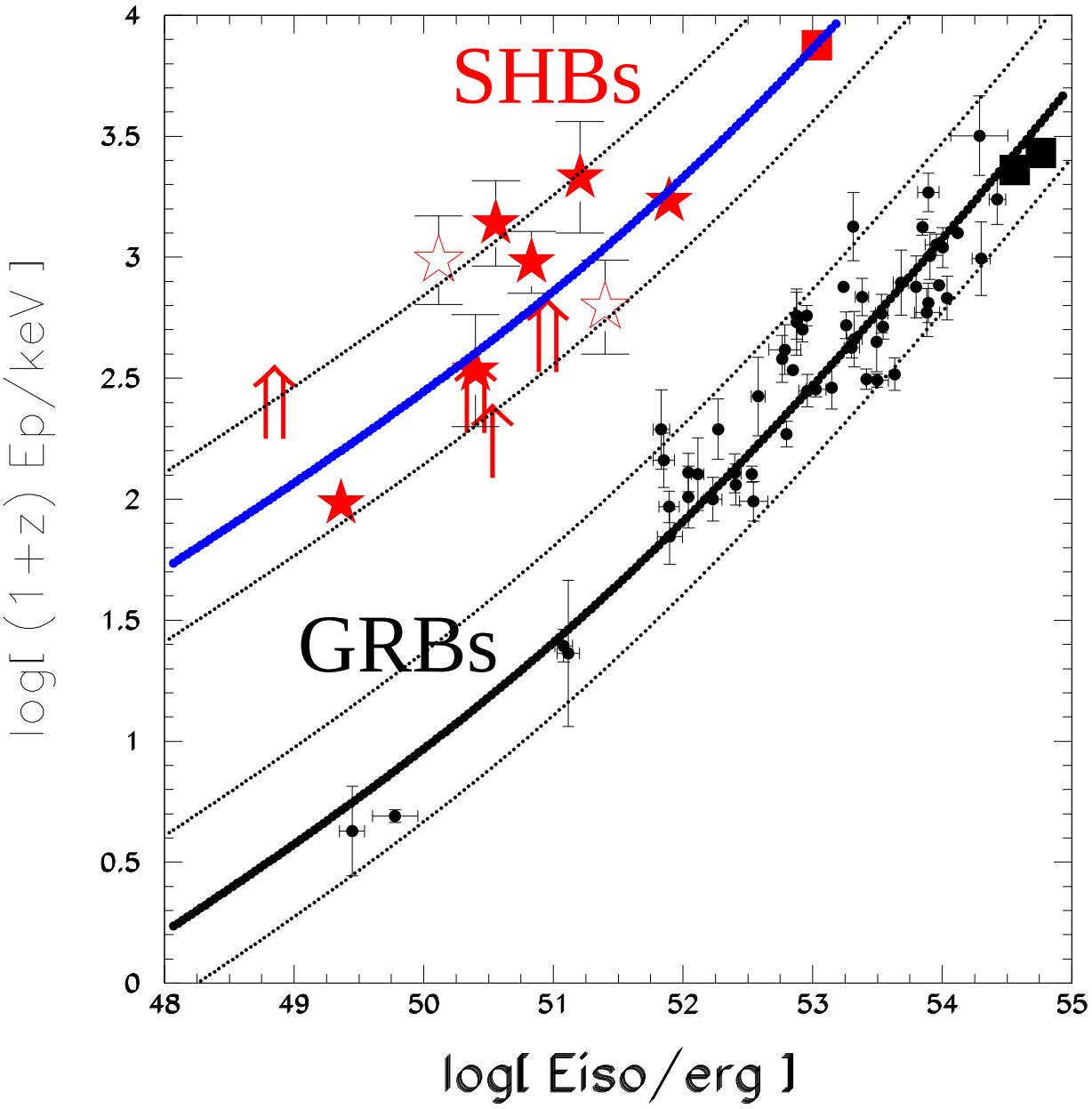

Fig. 2.— Comparison between the observed correlation [Ep,Eiso] in LGRBs and SHBs and the predicted correlation for LGRBs (DDD2007, Eq.(4)) and SHBs (DDD2009b, Eq.(22)). GRB 080916C, GRB 090902B and SHB 090510 are indicated by full squares (black, black and red, respectively, in the color version).

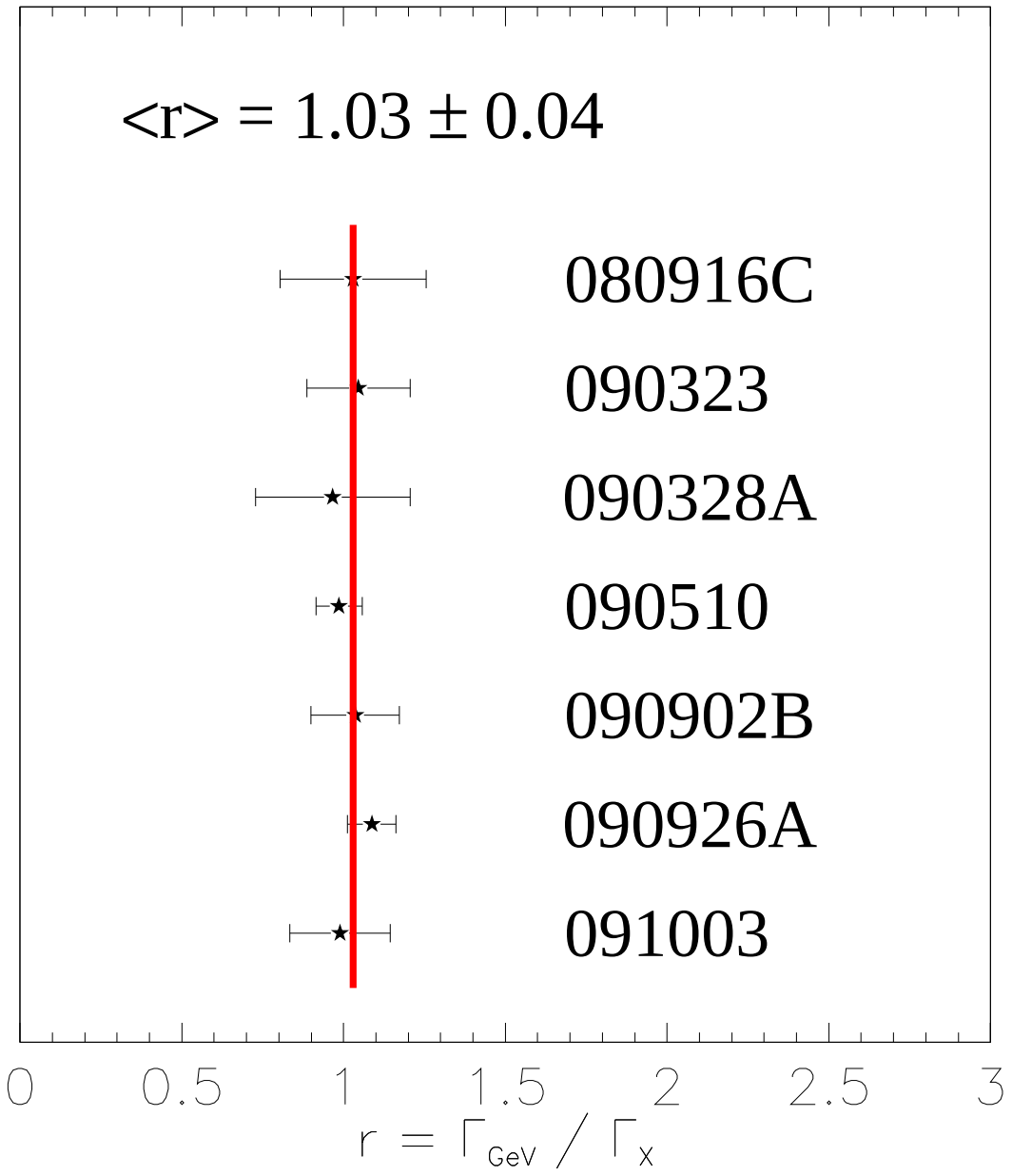

Fig. 3.— The ratio of the photon spectral index of the prompt HE emission detected by the Fermi LAT in several GRBs and the spectral index (Ghisellini et al. 2009) of their unabsorbed late-time X-ray AG inferred from the Swift XRT measurements and reported in the Swift Lightcurve Repository, Evans et al. 2009.

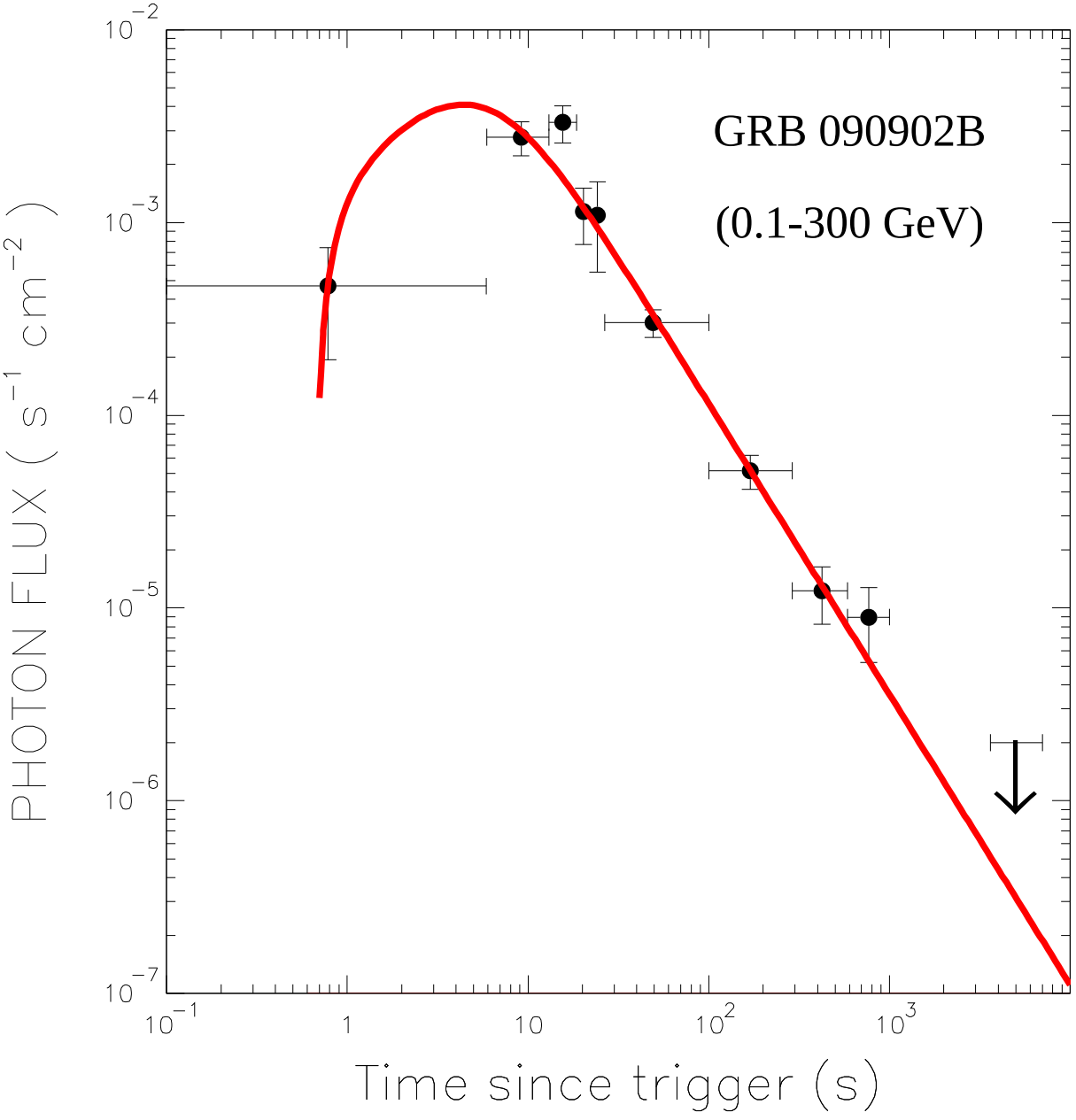

Fig. 4.— Comparison between the FERMI LAT lightcurve of the high energy emission in GRB 090902B (Bissaldi et al. 2009) and its CB model description, Eq. (**??**).

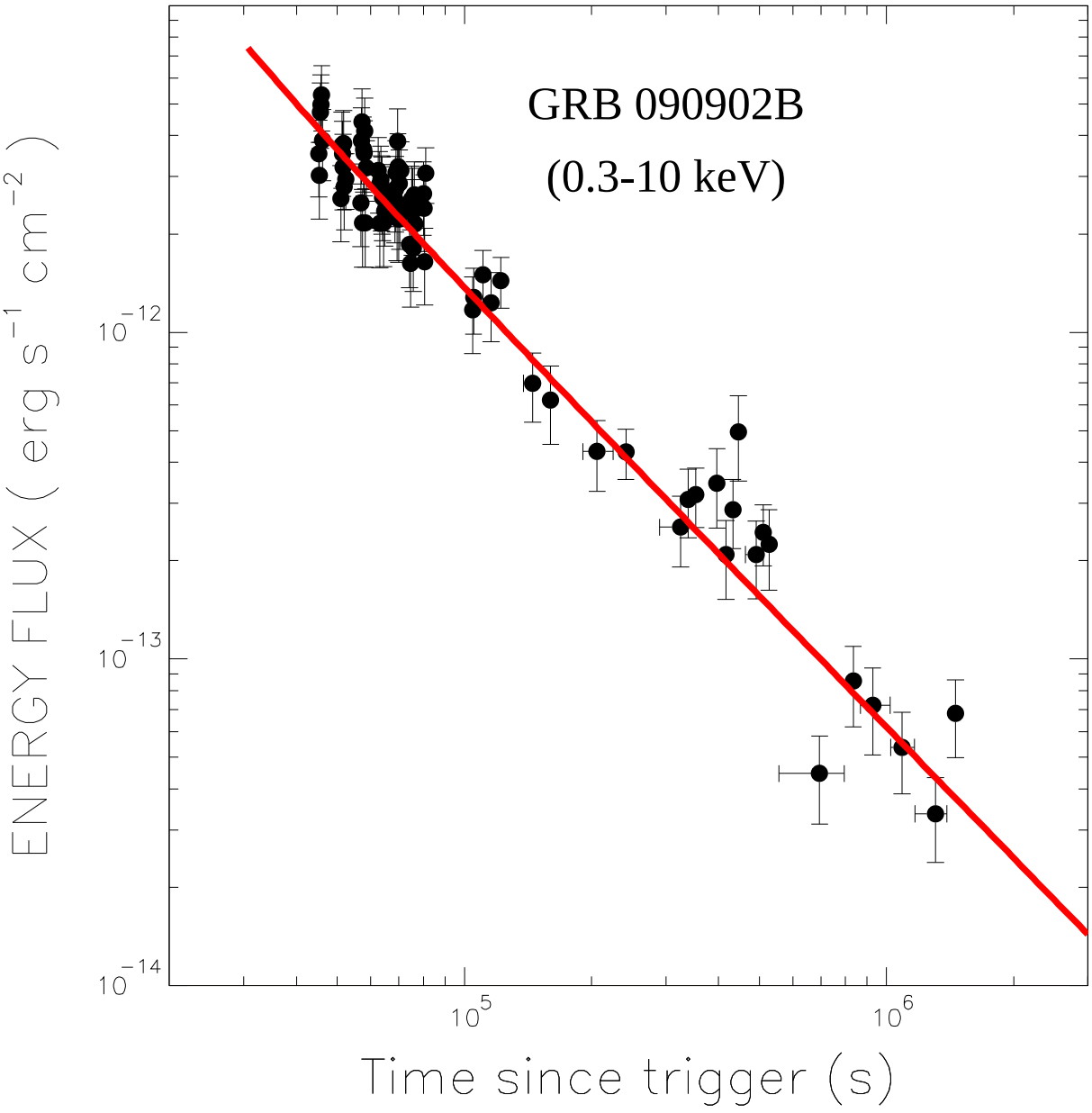

Fig. 5.— Comparison between the Swift XRT lightcurve of GRB 090902B (Evans et al. 2009) and its CB model description The asymptotic power-law decline with $\alpha_X = 1.42 \pm 0.10$ and $\beta_X = 1.10 \pm 0.30$ satisfies the CB model prediction $\alpha_x = \beta_X + 1/2$ for a constant density ISM.

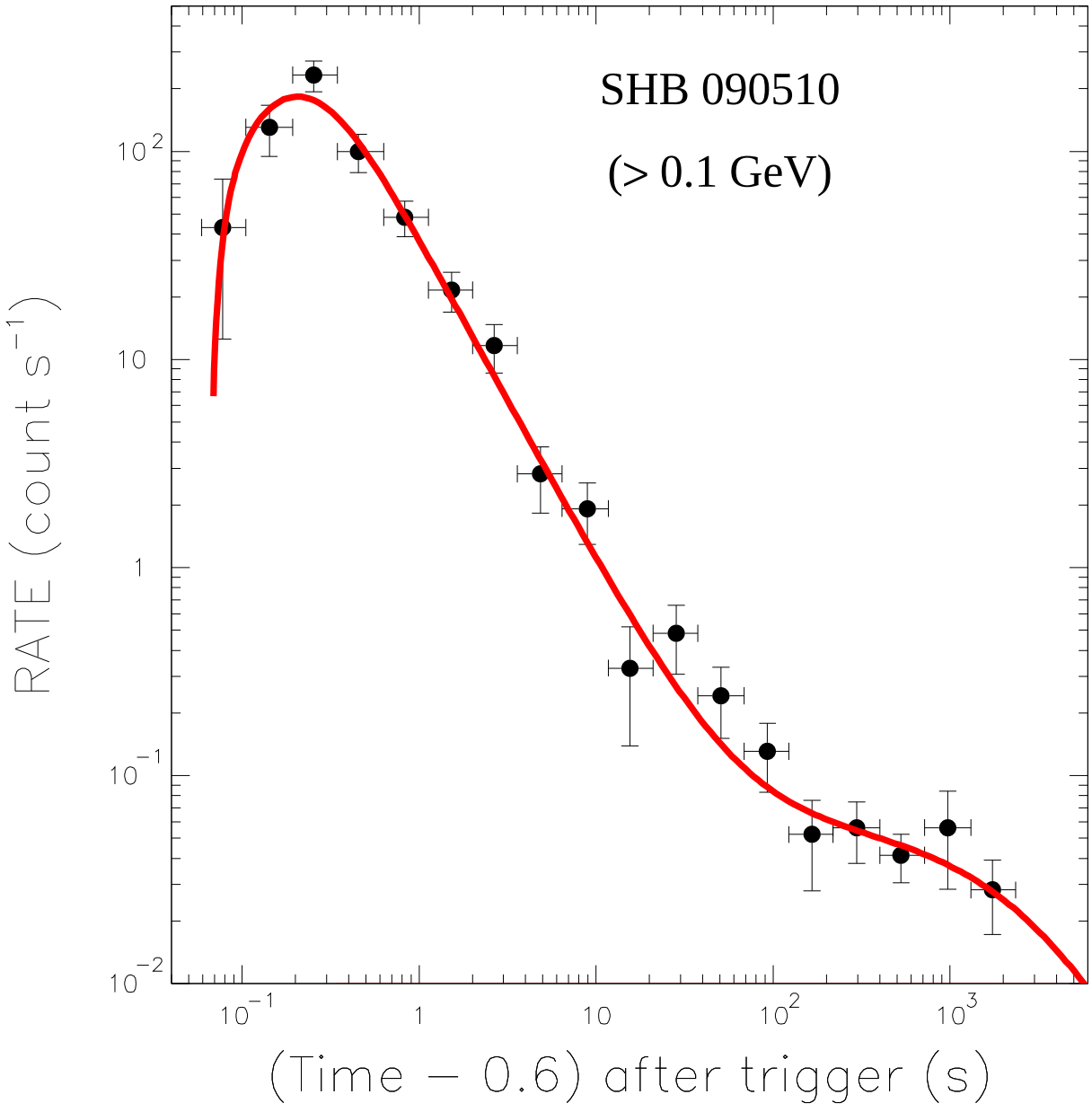

Fig. 6.— Comparison between the FERMI LAT lightcurve of the high energy emission in SHB 090510 (Ghirlanda et al. 2009) and its CB model description as given by Eq. (**??**).

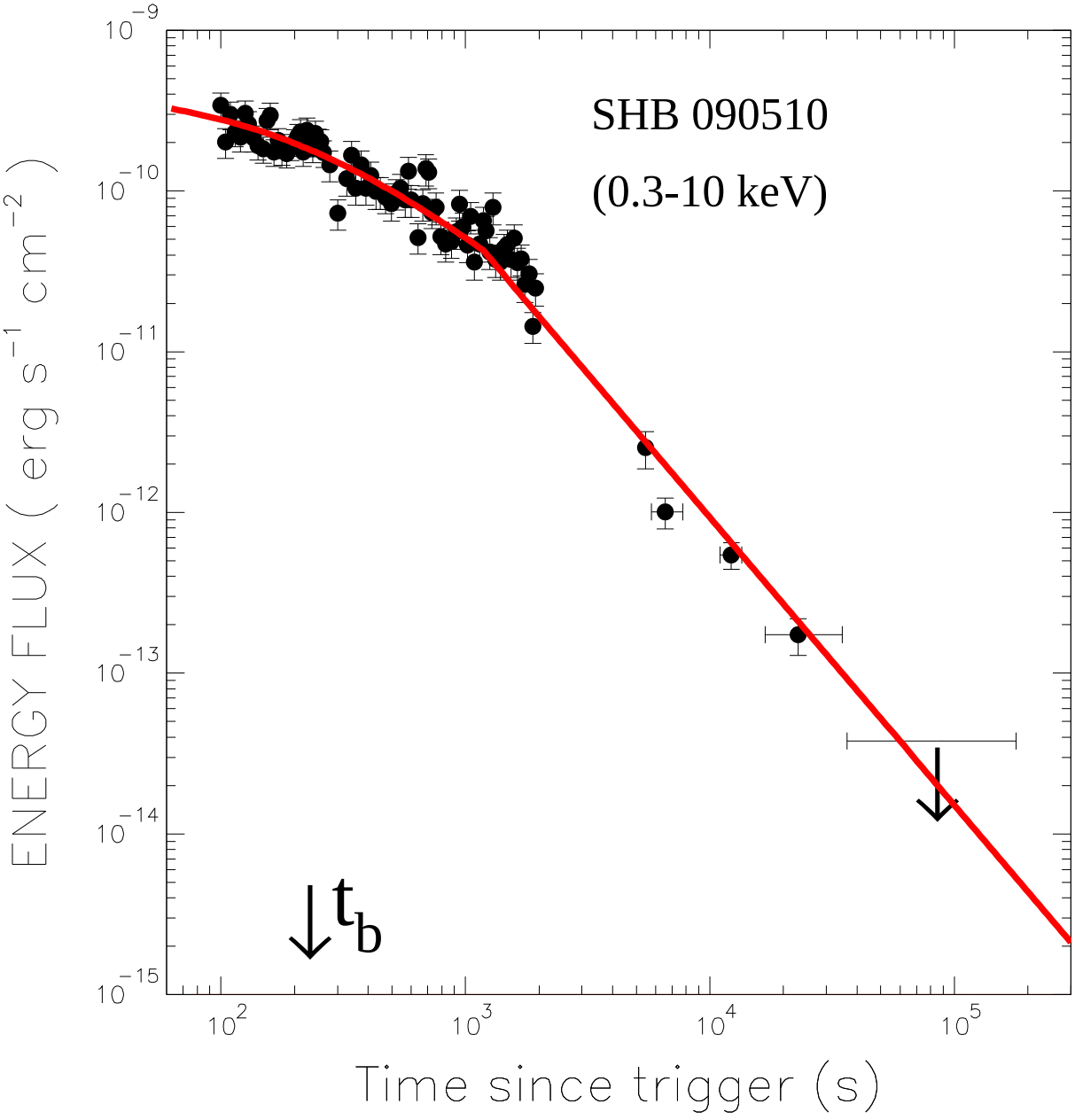

Fig. 7.— Comparison between the Swift XRT lightcurve of SHB 090510 (Evans et al. 2009) and its CB model description. The asymptotic power-law decline with $\alpha = 1.89 \pm 0.06$ and $\beta = 0.792(+0.71/-0.051)$ satisfies within errors the CB model prediction $\alpha = \beta + 1 = \Gamma$ for a density profile $n \propto 1/(r - r_c)^2$ beyond r_c (see DDD2009a,b).